Sustainable Energy & Fuels

ROYAL SOCIETY OF CHEMISTRY

PAPER

View Article Online
View Journal

Check for updates

Cite this: DOI: 10.1039/d5se01709b

Genome-resolved insights into Ni/Fe_2O_3 nanocatalyst-enhanced dark fermentative hydrogen production from food waste

Puranjan Mishra,[a] Ruilong Zhang,[a] Peixin Wang,[a] Yiqi Geng,[a] Dongyi Li,[ab] Qiuxiang Xu,[b] Jonathan W. C. Wong[b] and Jun Zhao *[ac]

Received 27th December 2025
Accepted 12th March 2026

DOI: 10.1039/d5se01709b

rsc.li/sustainable-energy

Ni/Fe_2O_3 nanocatalysts are effective in increasing the yield of fermentative biohydrogen (H_2); however, the underlying microbial and metabolic mechanisms remain insufficiently understood. In this study, food waste (FW)-based dark fermentative (DF) H_2 production was significantly improved by the addition of a synthesized Ni/Fe_2O_3 nanocatalyst, achieving an increase in H_2 yield up to 55.65% compared with that in the control. The presence of Ni/Fe_2O_3 enhanced the pH stability, conductivity, and electron transport capacity of the system, thereby simultaneously accelerating the microbial metabolism in the DF system. Genome-centric metagenomic analysis revealed that the catalyst reshaped the microbial community and metabolic functions by promoting *Clostridium* species as the dominant H_2-producing bacteria and enriching the genes associated with carbohydrate metabolism, complex saccharide hydrolysis, nutrient transport, glucose phosphorylation, and electron transfer pathways. These findings uncover a previously unrecognized catalytic role of Ni/Fe_2O_3 in regulating the microbial community structure and metabolic pathways, providing genome-level insights into catalyst–microbe interactions and offering a mechanistic foundation for advancing food waste-derived H_2 production.

1. Introduction

Global carbon emissions are driven by the widespread use of fossil-based fuels to meet the energy demand of the growing world population, intensifying the research attention towards sustainable bioenergy production.[1] The adoption of an integrated system combining the dark fermentative (DF) biohydrogen production with the advancement in nanotechnology to enhance the fermentative process is essential for achieving higher bioenergy production. Hydrogen (H_2), with its high calorific value (120–142 MJ kg^{-1}), is regarded as a green and sustainable fuel, and hence, the approaches to produce H_2 from biomass have become a significant area of research focus due to its potential for increasing the bioenergy efficiency and sustainability.[2] Leveraging the integration of materials nanotechnology and DF technology,[3] the biological conversion of nutrient-rich organic waste such as food waste[4] (which contains almost 30% of organics, *e.g.* complex polysaccharides, proteins, and lipids, and assures its regular generation of more than 2000 t per day (ref. 5)) into H_2 has immense potential to increase resilience and sustainability.[6]

H_2 production, in particular *via* DF from FW, primarily involved the 'solubilization' and 'hydrolysis' of macromolecules into monosaccharides and amino acids. Later, biologically, they got converted into acetate (C_2-H_{Ac}), butyrate (C_4-H_{Bu}) and other short-chain volatile fatty acids (VFA) with the simultaneous production of H_2 depending on the metabolic pathways followed by microorganisms (pyruvate-ferredoxin oxidoreductase pathway (PFOR) or pyruvate-formate lyase pathway (PFL)).[7] Although the DF process is ubiquitous and occurs in both natural environments and engineered systems,[8] the conversion of the complex organic macromolecules into H_2 remains challenging due to the low yield and productivity (as per the "Thauer limit", 4 mol of H_2 can be produced per mole of $C_6H_{12}O_6$ consumed).[9] The DF system has several significant environmental benefits in the production of H_2, and thus, numerous efforts have been dedicated previously to promote the H_2 metabolic process performance.[10] Engineered metallic nanoparticles have demonstrated enhanced electrocatalytic activities,[11] making them highly effective in the anaerobic processes aimed at optimizing the biological degradation of organic waste.[7] Metallic catalysts exhibit excellent catalytic activities to promote the DF-based bioconversion of waste into H_2 (by facilitating hydrolysis, improving solubility, and enriching hydrolytic bacteria within the microbial community).[12] In recent years, a series of metallic catalysts including metal oxides and

[a]*Sino-Forest Applied Research Centre for Pearl River Delta Environment, Department of Biology, Hong Kong Baptist University, Hong Kong, China. E-mail: zhaojun@hkbu.edu.hk*

[b]*Research Center for Eco-Environmental Engineering, Dongguan University of Technology, Dongguan, Guangdong 523808, China*

[c]*Institute of Advanced Materials, Hong Kong Baptist University, Hong Kong, China*

their derivatives have been explored to accelerate the H_2 production and microbial metabolic pathways,[7,13] and the quest to find a suitable nanocatalyst is expanding exponentially. Previous investigations have revealed the stimulating effect of single metallic nanoparticles on DF-based H_2 production and found that a connection exists among the type, size and exposure forms of nanoparticles.[14] These catalysts enhance the DF process performance in the following manner: (a) influencing the production activities of vital hydrogenase enzymes,[15] (b) facilitating the electron transfer between electron carriers,[16] (c) facilitating the substrate biodegradability,[17] and (d) facilitating cytoprotective properties of anaerobes.[18]

Considering the incorporation of the nanocatalyst, a significant enhancemnet in DF-system compared to the bulk one is being reported in literatures, which is attributed to their quantum size variations and high surface area, which ultimately increases electron adsorptions, efficient electron exchange between the catalysts and DF-system's microbial enzymes activities (NAD, FAD *etc.*).[19] Exemplifying this, iron, which is a vital element for enzymes (such as in [Fe–Fe] hydrogenases, [Fe–Ni] hydrogenases, dehydrogenases, and reductases), has been reported for its nanosized form for the catalytic activity in DF-based H_2 production systems.[20] The function of the nanocatalyst as a reducing agent lowers the oxidation–reduction potential (ORP) of the system and considerably enhances the hydrolysis of organic waste by fostering the anaerobic microenvironment of the DF system.[20] The efficacy of Fe-NPs have been explored in DF-system and presumed their catalytic functions relying on the shifting of intermediate metabolites production towards a higher C_2-H_{Ac} to C_4-H_{Bu} ratio, which favours increased H_2 production.[21] The morphological study of the catalyst reported the higher cell aggregation in the presence of Fe_2O_3 NPs due to the formation of bacterial nanowires, which played an important role in the electron transfer system during DF.[22] Nickle (Ni), a critical element which play an important role as cofactors of hydrogenase enzymes catalyzes energy based metabolic pathways, and availability of its adequate concentration elevate microbial growth and thereby H_2 productivity.[23] Study shows, the Ni/FeO_x nanoparticles has a bulk oxido-reductive potential as high as high 1.2 S^{-1} at an overpotential of 300 mV, while the higher catalytic activity of Ni/FeO_x is well established,[24] there is vivid debate like the activity, especially whether Ni/FeO_x is an active catalyst for H_2 production in DF-system. Zang *et al.*, reported that *Eichhornia crassipes's* extracted NiO NPs possess the ability to improve the H_2 productivity by 47.29% compared with control in DF-system.[25] Hydrogenase, a key enzyme of the DF-system that catalyzes NADH metabolism, can be categorized into [Ni–Fe] and [Fe–Fe] hydrogenases, which possess Fe and Ni as central active metal, and the former was more ubiquitous in microbes than the latter.[26] Ferredoxin, another important catalytic enzymes for H_2 generation in DF-system, Yang *et al.*[27] and Li *et al.*[23] reported the active participation of Fe and Ni composite in boosting which boost the synthesis of ferredoxin enzymes in DF-system.

The DF system-based H_2 production, which is associated with microbial functional dynamics, is complex, and still has a long way to go to become a competitive biofuel technology for H_2 generation at the commercial level. Although studies have been reported on the modulating effects of nano-sized catalysts on H_2 production *via* the DF system,[28] the use of bimetallic NPs and their cross-microbial dynamics and performance are yet to be explored, particularly in the systems augmented with Ni/Fe_2O_3 nanocatalysts.

Besides, the comprehensive analysis of the mechanisms underlying the Ni/Fe_2O_3 catalyst in microbial populations while using real FW in the DF system remains unexplored. Therefore, understanding the mode of action of Ni/Fe_2O_3 in the DF system using high-throughput metagenomics can give a clear picture of the Ni/Fe_2O_3-induced regulatory mechanism of the complex microbiome system followed by the pathways involved in the cellular process and organismal functions, but the metabolic pathways still need to be explored. The purpose of this study was to provide new taxonomic and metagenomic insights into the bioconversion of FW to H_2, specifically examining the microbial response to a prepared Ni/Fe_2O_3 catalyst in a DF-system. This study commenced with the synthesis of a novel Ni/Fe_2O_3 composite designed to improve the efficiency of H_2 production from FW in a DF-system. Subsequently, the physicochemical characteristics of the catalyst were comprehensively analyzed using X-ray diffraction (XRD), X-ray photoelectron spectroscopy (XPS), field emission scanning electron microscopy (FESEM), and transmission electron microscopy (TEM). The performance of the Ni/Fe_2O_3 catalyst was then systematically evaluated within the DF-system. This evaluation focused on: (a) the catalyst's influence on the hydrolysis and solubilization of FW; (b) its effect on the metabolic pathways for H_2 production, including volatile fatty acid (VFA) profiles and electron transfer system activity; and (c) its impact on microbial community dynamics. The latter was investigated through taxonomic and metagenomic analyses to elucidate the underlying genetic factors responsible for the catalyst's enhancement of H_2 production.

2. Material and methods

2.1 Catalyst preparation

The Ni/Fe_2O_3 NPs were prepared (on a molar ratio basis) by a modified co-precipitation method previously reported in the literature.[28] The procedure to prepare the catalyst in an aqueous iron nitrate nonahydrate solution is as follows: in 100 mL of H_2O, 0.1 mM Fe $(NO_3)_3 \cdot 9H_2O$ (Sigma-Aldrich) and 0.05 mM of Ni $(NO_3)_2 \cdot 6H_2O$ (Sigma-Aldrich) were fully dissolved under continuous stirring, followed by precipitation by the dropwise addition of 1 M NaOH (adjusted till pH 10–11). Upon pH adjustment, the reaction mixture was seeded by heating to 80 °C with stirring (450 rpm) for 3 h. The resulting slurry was properly deionized with H_2O and ethanol; and then, the slurry was dried at 60 °C for 16 h to allow the complete evaporation of water. The resulting material was ground prior to calcination (450 °C, 2 h, 5 °C min^{-1}).[28]

2.2 Catalyst characterization

The structure of the catalyst was determined by power X-ray diffraction using a Cu Kα radiation source, at 40 keV and 40 mA. X-ray photoelectron spectroscopy was performed to analyze

the composition and redox states of catalysts, and the atom distribution was observed using TEM-EDS analysis. The surface morphologies of the catalyst were studied using a field emission scanning electron microscope (FESEM, Zeiss) operating at an electron voltage of 5 kV. A transmission electron microscope (TEM; tecnaiG2 FEI Co TEM) operating at an accelerating voltage of 200 kV was used to configure the internal morphologies.

2.3 Food waste and seed sludge

The substrate used was a synthetic FW prepared in the laboratory. Prior to each experiment, the FW was diluted with tap water and blended to form a slurry. This mixture was then adjusted to the final target values for Total Solids (TS) and pH. A complete list of the FW constituents is provided in the SI. For the inoculum prepration, the sludge was heat pretreated following the procedure mentioned in literature.[29] The sludge was taken from Sai Kung sewage wastewater treatment plant, Sai Kung, Hong Kong, and stored at 4 °C to prevent degradation. The characteristics of seed sludge and FW are mentioned in the SI (Section 1). For the enrichment of H_2-producing microbes and restraining methanogens, the sludge was incubated at 90 °C for 2 h in a water bath system.[28]

2.4 Role of Ni/Fe_2O_3 in the solubilization and hydrolysis of FW

The DF process using FW as the substrate is critically related to solubilization and hydrolysis.[12] Herein, the effects of solubilization and hydrolysis at various doses of Ni/Fe_2O_3 ranging from 50 to 500 mg L^{-1} were investigated using FW, where the DF lasted for 3 days. The detailed procedures are provided in the SI (Section 2(a and b), SI).

2.5 Role of Ni/Fe_2O_3 in DF system-based H_2 production from FW

An experiment was conducted on Ni/Fe_2O_3 affecting the H_2 production and microbial community at their metabolic and genomic levels using identical serum bottles with a working volume of 120 mL. The FW slurry with an initial TS of 10 g L^{-1} was prepared using tap water, and 10% heat-pretreated sludge[30] was added. The mixture was divided equally by 18 reactors, which belong to six groups with three samples each, to study the effect of H_2 production and microbial taxio-metagenomic analysis. Based on the Ni/Fe_2O_3 catalyst doses employed in the DF process, the reactors were labelled as control, T-50, T-100, T-200, T-300 and T-500 mg L^{-1} of Ni/Fe_2O_3, respectively. The initial pH of each serum bottle was adjusted to 5.5 ± 0.2. After flushing with nitrogen gas for 2 min to remove O_2, all the serum bottles were capped properly with a rubber stopper, sealed and placed in an orbital shaker at a speed of 180 rpm and an incubation temperature of 35 °C ± 2 °C for 3 days. The final pH and conductivity (E_h) were measured post DF. Liquid samples were collected from the serum bottles using a 5 mL gas syringe, filtered through a 0.2 μm membrane and stored in a 2 mL GC vial at 4 °C for physico-chemical analysis. Volumetric analysis of the produced H_2 gas was performed by measuring the head space, the fraction of H_2 in the gas composition in the head space, and the pressures exerted in each serum bottle.

2.6 Role of Ni/Fe_2O_3 catalysts in the electron transport system

To analyze the electro-catalytic behavior of Ni/Fe_2O_3 catalysts in the microbial activity during DF, the ETS activity was analyzed by performing a modified 2-(*p*-iodophenyl)-3-(*p*-nitrophenyl)-5-phenyl tetrazolium chloride (INT) assay.[31] In brief, after 4 days of fermentation in seven groups of identical reactors with corresponding levels of Ni/Fe_2O_3-5% (control, 50 mg L^{-1}, 100 mg L^{-1}, 150 mg L^{-1}, 200 mg L^{-1}, 300 mg L^{-1}, and 500 mg L^{-1}), the samples were collected from each reactor, and the electron transport system activity was determined. The detailed methodology to assess the ETS activity is mentioned in the SI (Section 2(c), SI).

2.7 DNA extraction, sequencing and bioinformatics analysis

To analyze the microbial communities, we selected the control group (no Ni/Fe_2O_3) and a representative experimental group (200 mg per L Ni/Fe_2O_3) that exhibited a high H_2 yield. For each group, 5 mL aliquots were collected from three parallel 3-day fermentation replicates, pooled into a composite sample, and stored at −80 °C. Total genomic DNA was extracted and quantified from each composite sample. The V4–V5 hypervariable region of the 16S rRNA gene was then amplified using PCR and sequenced. All procedures followed established methods from the literature.[32] The sequence content quality score across (Tables SA1–SA3, SI) all bases observed for the control and test samples are highlighted with detailed information on the sequencing and metagenomic analysis procedures in the SI (Section 2(d), SI). All the assays were conducted in triplicate, and the results are presented as error bar (±standard deviation). An analysis of variance (ANOVA) was used to test the significance of the results, and a p value of 0.05 was considered statistically significant.

2.8 Sampling, analysis and analytics

The total solids (TS), volatile solids (VS), and pH of the FW and sludge inoculum in the experiments were analyzed using APHA standard Method 2540.[33] The constituents of FW (C, H, N, and S) were analyzed using an ELEMENTAR Vario MARCO cube Analyzer (Sci Focus Lmt., Hong Kong). The conductivity of DF systems (pre and post fermentation) was measured using a Portable Digital lab Conductivity Meter Dds-11c (Puchun Instruments, Shanghai), in which the probe of the conductivity meter was calibrated using 0.01 M KCl, with 1413 μS cm^{-1} at 25 °C to ensure the authenticity of the observed conductivity. Fraction analysis of the produced gas was performed using a gas chromatography (GC-8500, Perkin, USA) equipped with a TCD detector, a column (SS350A) and a molecular sieve (80/100 mesh). The soluble metabolite analysis was performed by high-performance liquid chromatography (HPLC-Agilent-1200, USA). The operational conditions applied for GC and HPLC, and the calculation for the H_2 magnitude were referred from our previous experimental study.[28] Prior to soluble metabolite analysis, the samples from the ceased H_2 production system

were collected, centrifuged at 6000 rpm for 10 min and filtered through a 0.45 μM membrane.

3. Results and discussion

3.1 $NiFe_2O_3$ synthesis and characteristics

A brownish powdery mixture was obtained after the final calcination of the starting materials $Fe(NO_3)_3 \cdot 9H_2O$ and $Ni(NO_3)_2 \cdot 6H_2O$ with 0.01 mM iron precursor and 0.005 mM Ni precursor. The scanning electron microscopic images displayed in Fig. 1a–c show the crystalline morphologies in the nanosize ranges. The XRD patterns (Fig. 1g) of Ni/Fe_2O_3 show distinct diffraction peaks, which can be assigned to the (111), (200), (311), (400), (511), and (440) reflection crystal planes of the face-centered cubic nickel phase (JCPDS 54-0964). However, a light shifting at (220) and (311) corresponding to Fe_2O_3 (39-1346) in the Ni/Fe_2O_3 composite could be observed, implying the substitutional associations between iron and nickel particles.

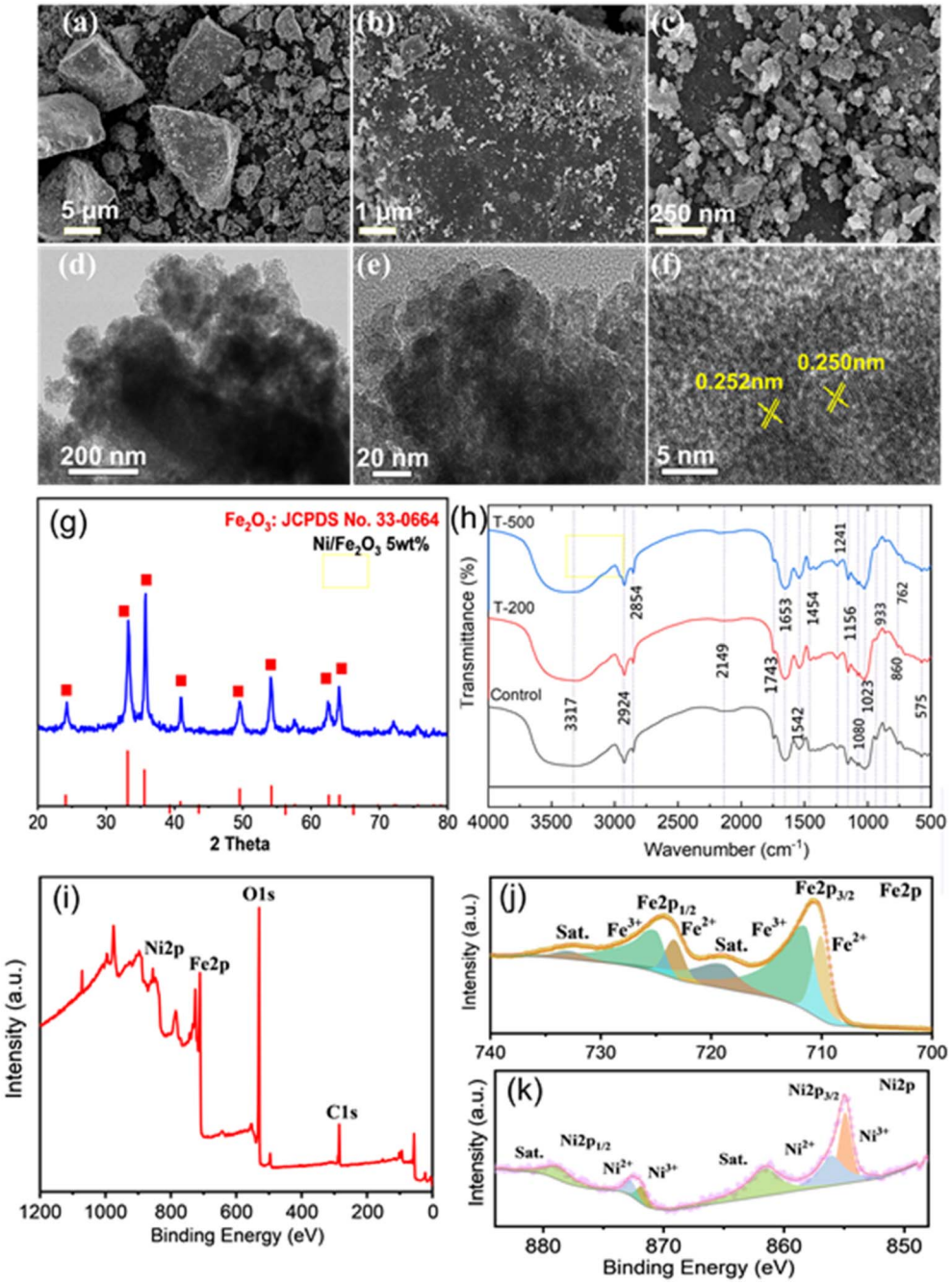

Fig. 1 (a and b) Low-magnification and (c) high-resolution SEM images of representative Ni/Fe_2O_3-5%. (d) Corresponding low-magnification and (e and f) high-resolution TEM images of Ni/Fe_2O_3-5%. (g) XRD spectrum of the representative Ni/Fe_2O_3-5% sample. (h) FT-IR spectrum of food waste sampled from post-anaerobic biohydrogen production enriched with and without Ni/Fe_2O_3. (i) Full XPS spectrum of the representative Ni/Fe_2O_3-5% sample. High-resolution XPS spectra of (j) Fe 2p and (k) Ni 2p.

The Scherrer analysis[28] of diffraction peaks (311) for Fe_2O_3 (39-1346) suggested a grain size of 0.251 nm at 2θ of 35.630, while the $Ni_{0.05}Fe_{0.1}$ composite indicated a grain size of 2.5130 nm along the 35.699 (2θ) crystallographic axis direction,[34] consistent with the results observed by SEM (Fig. 1c). The observed diffraction peaks illustrated that Ni/Fe_2O_3 catalysts have a proportion of crystalline regions, thus making the material more stable. The SEM images of Ni/Fe_2O_3 catalysts displayed in Fig. 1c show the appearance of irregularly agglomerated shapes. The particles were relatively uniform and smooth, and were slightly agglomerated.[35] Acquiring the elemental composition of Ni/Fe_2O_3, the XPS spectrum, shown in Fig. 1i–k, reveals the existence of Ni, Fe and O, and this is consistent with the XRD results, indicating the purity of the Ni/Fe_2O_3 catalysts. The XPS survey orbital spectrum peaks at 529, 780 and 855 eV confirmed the existence of O 1s, Fe 2p and Ni 2p, respectively.[23] The high-resolution TEM images of nanoparticles displayed in Fig. 1d–f present 0.250 lattice fringes, which can be attributed to the (311) lattice plane of the Ni–Fe composite,[36] in line with the XRD results. The XPS oxygen spectrum (Fig. S1, SI) reveals different oxygen components, labeled as O1, O2 and O3, respectively. O1 corresponds to the typical metal–oxygen bond in the oxides with a binding energy value of 529.6 eV, while O2 and O3 peaks at 530.9 eV and 532.7 eV correspond to oxygen vacancies.[37] These vacancies are important to resist the proton movement and acceleration of shuttling in the surface layer.[38] Further, the Ni 2p spectrum exhibited peaks at 854.8 eV and 872.6 eV of $2p_{3/2}$ and $2p_{1/2}$, respectively, depicting Ni^{3+} and Ni^{2+} (Fig. 1k), respectively. The refraction peaks at 854.8 eV and 856.3 eV are ascribed to Ni^{3+} and Ni^{2+} in the Ni $2p_{3/2}$ orbital. Similarly, the refraction peaks at 871.9 eV and 872.7 eV are ascribed to Ni^{3+} and Ni^{2+} in the Ni $2p_{1/2}$ orbital, which are in line with the results reported in the literature.[39,40] The Fe 2p profiles with two peaks at 710.8 eV and 724.4 eV for Fe $2p_{3/2}$ and Fe $2p_{1/3}$, respectively, indicated the presence of Fe^{2+} and Fe^{3+} (Fig. 1j). The peaks at 709.9 eV and 712 eV are ascribed to the presence of Fe^{2+} and Fe^{3+}, which coexist in the Fe $2p_{3/2}$ spin. Similarly, the refractive peaks at 723.2 eV and 725.5 eV are ascribed to the presence of Fe^{2+} and Fe^{3+}, which coexist in the Fe $2p_{1/2}$ spin.[41,42] The nature of charge on metal ions is critical for the systematic improvement in E_h of Ni/Fe in the system.[43] Based on the observed peak areas for Ni^{2+}, Ni^{3+}, Fe^{2+} and Fe^{3+}, the Ni/Fe_2O_3 catalysts exhibited bivalency with Ni^{2+}/Ni^{3+} and Fe^{2+}/Fe^{3+} ratios of 1.07 and 0.40, respectively.

3.2 Ni/Fe_2O_3 facilitated FW solubilization and hydrolysis

FW a complex substrate, the extent of its hydrolysis and solubilization is critical. This process disintegrates the FW into simple nutrients, releasing them into the liquid broth and enabling mass transfer to the microbial community. These steps are essential for significant H_2 production in the DF-system.[12] Fig. 2(a and b) depict the soluble protein and polysaccharide concentration after fermentation in response to

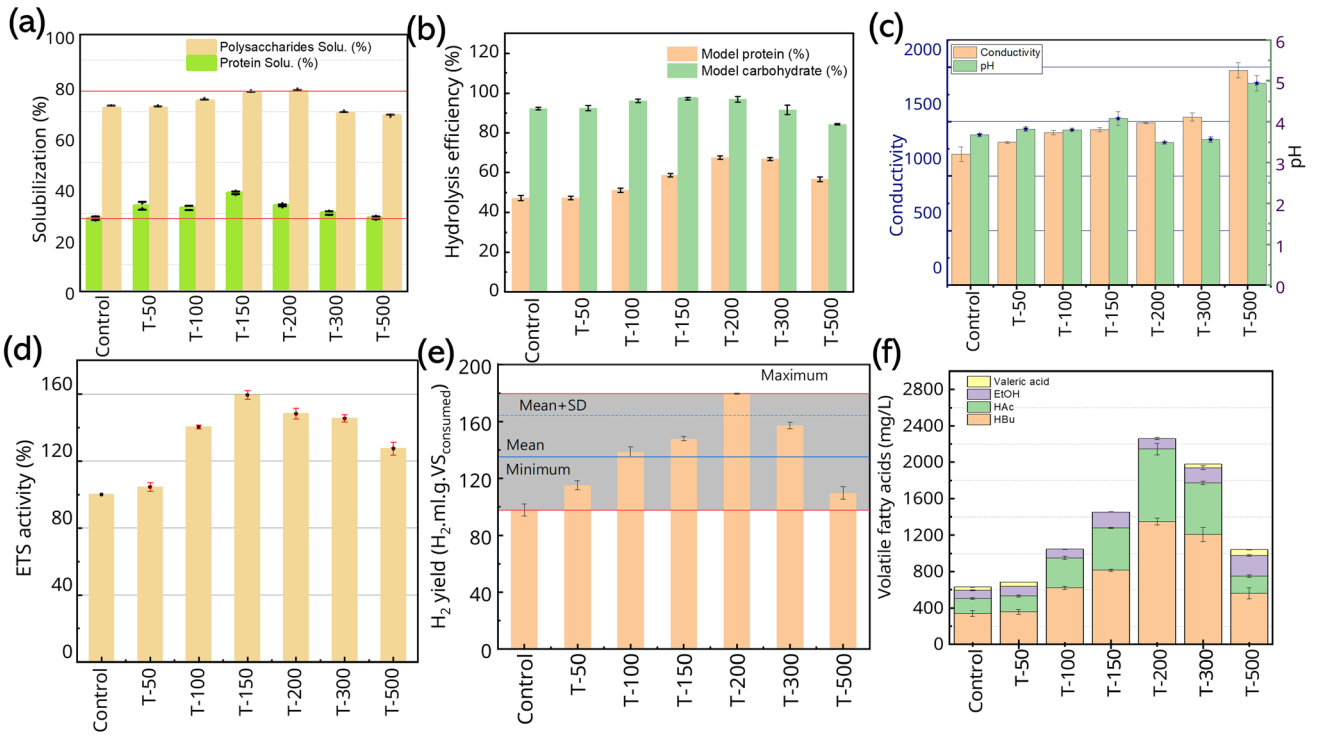

Fig. 2 (a) Solubilization profile of model polysaccharides and proteins after fermentation. (b) Hydrolysis efficiency profile of model proteins and saccharides as model compounds p^*, the sample test variance was statistically calculated using the one-sample Wilcoxon signed rank t-test (WSRT t-test). (c) Conductivity and pH profiles of the spent medium. (d) Electron transport system activity profile. (e) Hydrogen yield profile. (f) Soluble metabolite profile.

different concentrations of Ni/Fe_2O_3 added to the FW-based DF system. In Fig. 2a, at the Ni/Fe_2O_3 level of 50, 100, 150, 200, 300 and 500 mg L^{-1}, the soluble polysaccharide concentration was 71.26%, 74.15%, 77.25%, 77.91%, 65.62%, and 65.98%, showing significant variations ($p = 0.02$, $p < 0.05$), whereas compared with the control (71.23%), the test-medium with 200 mg L^{-1} of Ni/Fe_2O_3 appeared to be increased by 7%, indicating that more soluble carbohydrates are released into the DFHP system. A similar trend was observed for soluble protein analysis, where, at the Ni/Fe_2O_3 level of 50, 100, 150, 200, 300 and 500 mg L^{-1}, the soluble protein concentration was 32.96%, 32.11%, 38.06%, 33.17%, 30.19%, and 28.28%, showing a significant variation in concentrations ($p = 0.02$, $p < 0.05$). The addition of 200 mg L^{-1} of Ni/Fe_2O_3 to the DF-system increased protein solubility to 30.88%. This represents a 10% increase compared to the control system (28.07%). Hydrolysis of FW refers to the degradation of polysaccharides (macro molecular saccharides) and soluble protein into monosaccharides and amino acids, respectively.[44] Fig. 2b shows the degree of hydrolysis in % using BSA and cellobiose as the model protein and carbohydrate in response to different dosages of Ni/Fe_2O_3 ranging from 50 mg L^{-1} to 500 mg L^{-1} in the DF system after 3 days of incubation. In the control system, where no Ni/Fe_2O_3 was added, the content of BSA and cellobiose during hydrolysis was observed as 47.25% and 92.24%, respectively. This suggests that the anaerobic sludge contains a considerable amount of microbiomes able to hydrolyze the complex low-molecular disaccharides. The decline in the degree of food waste hydrolysis observed at Ni/Fe_2O_3 nanoparticle concentrations above 300 mg L^{-1} can be explained by two primary factors. First, at high concentrations, the nanoparticles exert a toxic effect on hydrolytic bacteria, inducing significant oxidative stress that damages essential cellular components like DNA, proteins, and cell membranes.[45] Second, the nanoparticles act as strong reducing agents, and an excessive dose can drastically lower the system's redox potential beyond the optimal range for the microbial community, causing a metabolic shock and inhibiting their activity.[46] These observations are consistent with the phylum-level microbial diversity analysis where *Bacillus* sp. was the second dominant species after *Clostridium* species (later discussed in the section metagenomic analysis). Although it was observed that the degradation efficiency of cellobiose and BSA increased from 92.25% to 97.24% ($p < 0.05$) and 47.25% to 66.88% ($p > 0.05$), respectively, the protein hydrolysis efficiency shows a variation due to the presence of Ni/Fe_2O_3. The hydrolysis facilitates the cleavage of bonds in complex polysaccharides, proteins, and lipids. Herein, a variation in the abundance of genes encoding for a group of enzymes such as esterase (EC: 3.1.1), which acts on the ester bond on complex lipids, glycosidases (EC: 3.2.1) facilitate the hydrolysis of *O*- and *S*-glycosyl bonds and proteases (EC: 3.4) were further investigated through COG and NOG, analysis, as discussed in Section 3.4. These observed variances in gene abundances participating in hydrolysis signify and strengthen the overall catalytic role of Ni/Fe_2O_3 that improves the hydrolysis of complex FW compared with the control one by stimulating the hydrolytic efficacy of microbial consortium.

Nano Ni/Fe_2O_3 exhibits surface active ions and can interact with organic matter in both aqueous and non-aqueous phases, which might cause ionic and non-ionic interactions between hydrophilic organics such as those in food waste.[47] Besides, the biological interaction of Ni/Fe_2O_3 catalysts and the essential enzymes responsible for hydrolysis and solubilization results in an increased production of hydrolytic enzymes, evidenced by metagenomic analysis. Similar reports on nano catalysts and FW have suggested that the Fe_2O_3 and NiO nanoparticles enhanced the activity of enzymes associated with hydrolysis, such as proteases and alpha glycosidase in the anaerobic biohydrogen process.[48,49] Fourier transform infrared (FTIR) spectrum was used for the assessment of various functional groups resulting from the presence of Ni/Fe_2O_3 in the FW-based DF system, as shown in Fig. 1h. This FTIR spectroscopic assessment was performed for the samples taken from the FW DF system, labeled as control, and the system added with 200 mg L^{-1} and 500 mg L^{-1} of Ni/Fe_2O_3 catalyst. The observed elongated peaks at 3000–3500 cm^{-1}, were attributed to the O–H stretching vibrations, indicating the presence of water or hydroxy groups in the post-fermentative FW-based DF system. In the spectrum, the concomitant appearance of peaks at 2924.76, 1653.62, 1156.55, 1241.07, 1053.50, 933.49, and 765.74 cm^{-1} corresponded to C–H stretching vibrations, C=O and C=C vibrations, C–O–C and C–O stretching vibrations, C–O-R stretching vibrations, S–O stretching vibrations, O–H bending vibrations (carboxylic acids) and *cis* =C–H vibrations, respectively (Table S1, SI), confirming the intercalations of aliphatic methylene groups, aldehyde–carboxylate–aromatic skeletons, polysaccharides–phosphodiesters, inorganic sulfates, ether units, carboxylic acids and alkyl halides in the post-fermented FW from the DF system.[50] The infrared peak of 1156 cm^{-1} (aromatic amines) was observed to be higher in the samples added with Ni/Fe_2O_3 than in the control one. Besides, fluctuations in the infrared peak at 921.49 cm^{-1} were observed. Particularly, the decreased infrared peak at 1156.55 cm^{-1} (polysaccharides) and 933.49 cm^{-1} (VFA) indicates the consumption of mono-molecules dissociated from the macromolecules and their subsequent degradation. The FT-IR behavior of this band is slightly different from the FW sample added with Ni/Fe_2O_3, and it might be attributed to the released metabolites in samples, and enough to become visible in the spectrum, which signifies the enriched H_2 yield.

3.3 Ni/Fe_2O_3-mediated FW-based DF biohydrogen production

The effects of Ni/Fe_2O_3 on key system parameters—specifically pH, E_h, and H_2 production performance—in the FW-based DF-system are presented in Fig. 2c. The maximum E_h value of 1971.5 mS m^{-1} was detected in the fermentation system containing 500 mg L^{-1} of Ni/Fe_2O_3. Compared with the controlled DF system (1202.5 mS cm^{-1}), the observed magnitude of E_h variation is significant ($p < 0.05$). This can be attributed to the uniform dispersion of the nanoparticles. When properly applied, the high redox potential of the composite material is transferred to the biological system, thereby enriching the

overall fermentation environment. The redox-active nature of nanomaterials like Ni, Fe_2O_3, and their composite contributes to an increased E_h in the DF-system. These materials may act as electron conduits, enhancing electrochemical activity. The pH of the DF system, as depicted in Fig. 2c, is a crucial indicator, revealing the metabolic shifting as well as microbial population shifting biosystems. The fluctuation in the pH of the spent medium was observed in response to the varying concentration of Ni/Fe_2O_3. The pH in the DF-system supplemented with 500 mg L^{-1} of Ni/Fe_2O_3 increased to 4.9, compared to 3.67 in the control. However, this increase was not statistically significant ($p > 0.05$).

The relationship between the E_h value and the ions for the DF-based biohydrogen process is well known ($G = a \times H_{ac} + b \times H_{bu} + c \times Na^+ + d \times HCO_3^- + G_0$, where Na represents the sodium ion concentration for a particular pH to regulate the system pH).[51] Focusing on the H_2 yield of the hydrogen production system, at levels of 200 mg L^{-1} of Ni/Fe_2O_3 to the system, the pH of the ceased DF system varied from 3.61 to 3.49 and E_h from 1202.5 to 1428.5 mS^{-1}. This evidence indicates that applying Ni/Fe_2O_3 nanoparticles to the DF-system is beneficial, likely due to the release of redox-active ions (Ni^{2+}/Ni^{3+} and Fe^{2+}/Fe^{3+}). These nanoparticles appear to regulate the system's environment, significantly altering the pH and lowering the conductivity compared to the control.[52] This leads to an increase in H_2 production, which is consistent with the existing literature, indicating that a reduction in system pH can enhance the H_2 productivity.[27,53] The activity of the ETS was determined to assess the overall metabolic rate of the microbial community. This assay measures the activity of dehydrogenase enzymes, which catalyze the initial steps of electron transfer in anaerobic respiration.[54] The conducted ETS assessment shows the change in microbial metabolic activity in response to Ni/Fe_2O_3 in the DF system. As shown in Fig. 2d, the ETS activity is positively correlated with the Ni/Fe_2O_3 doses, which is consistent with the production performance of H_2. The addition of Ni/Fe_2O_3 significantly ($p < 0.05$) enhanced ETS activity compared to the control across all tested concentrations. The effect peaked at 150 mg L^{-1} with a 59.45% increase, while other concentrations (50, 100, 200, 300, and 500 mg L^{-1}) resulted in increases of 4.37%, 40.37%, 48.21%, 45.48%, and 27.42%, respectively. The trace metal ions have specific biochemical functions in the cell during the ETS-associated metabolic pathways, and any change in its concentration alters the metabolic function. Herein, the presence of Ni^{2+}/Ni^{3+} and Fe^{2+}/Fe^{3+} in Ni/Fe_2O_3 increased the potential for metabolic activity, which is coordinated with the electron transport system. The presence of 150 mg per L Ni/Fe_2O_3 in the DF system increases the electron transport activity up to 59.45% compared with the control. A possible explanation is that Ni^{2+} and Fe^{2+} ions act as electron mediators, promoting ETS activity through multiple mechanisms in the DF-system. Their presence is maintained by the reduction of Fe^{3+} to Fe^{2+} and Ni^{3+} to Ni^{2+}.[55,56]

Increments in the H_2 yield in the DF system in response to different dose levels of Ni/Fe_2O_3 were observed, which are depicted in Fig. 2e. The H_2 yield increased to 179.62 H_2 mL per g of $VS_{consumed}$ when the DF system was supplemented with 200 mg L^{-1} of Ni/Fe_2O_3, whereas the system added with Ni/Fe_2O_3 > 200 mg L^{-1} showed a lower H_2 yield. In the controlled DF system (no Ni/Fe_2O_3 added), a H_2 yield of 97.57 H_2 mL per g of $VS_{consumed}$ was observed. The supplementation of Ni/Fe_2O_3 to the DF system, significantly ($p < 0.05$) increased the H_2 yield, and as the doses of Ni/Fe_2O_3 increased from 50 to 200 mg L^{-1}, the H_2 yield increased from 115.09 to179.62 H_2 mL per g of $VS_{consumed}$, which was an increase of 55.65% compared with the control. At higher concentrations, an inhibitory effect was observed. Specifically, as the Ni/Fe_2O_3 dosage increased from 200 to 500 mg L^{-1}, the H_2 yield dropped from 179.62 to 109.63 H_2 mL per g of $VS_{consumed}$. This decline indicates a suppression of microbial metabolic activity. The increased H_2 yield is likely due to the ability of DF bacteria to adapt to the Ni/Fe_2O_3-amended environment. The nanoparticles serve as electron mediators, altering microbial electron transfer in a way that enriches metabolic pathways. This process increases the NADH/NAD^+ and $FADH_2$/FAD ratios and stimulates the production of extracellular polymeric substances, ultimately boosting H_2 production.[57] The unique adaptive ability of the microbial community to Ni/Fe_2O_3 nanoparticles is central to the enhanced growth and H_2 generation observed. This adaptation, which is dependent on nanoparticle concentration, is supported by genomic evidence. We detected an increased abundance of key COGs, particularly those for hydrolase, FMN- and NAD-oxidoreductase, and electron transport system enzymes. The upregulation of these genes directly impacts cellular bioenergetics by influencing ATP and H^+ gradient formation, which in turn regulates the [Fe–Ni] hydrogenases essential for H_2 production in the DF-system. Soluble metabolite analysis suggested that, when the dosage of Ni/Fe_2O_3 in the DF-system increased from 50 to 200 mg L^{-1}, the C_2-H_{Ac}/C_4-H_{Bu} ratio increased from 0.49 to 0.58 (Fig. S2), while with the further increase in doses of Ni/Fe_2O_3 to 500 mg L^{-1}, the ratio decreases to 0.33. All the test groups exhibited a comparable molar ratio of C_2-H_{Ac}/C_4-H_{Bu} ranging from 0.490 to 0.586 and dominated proportion of C_4-H_{Bu}. The higher concentration of C_4-H_{Bu} over C_2-H_{Ac} in the DF system, suggests the 'butyrate type of hydrogen production' metabolic pathway followed by microbial population.[28,58]

The DF system with Ni/Fe_2O_3 (200 mg L^{-1}) exhibited a higher C_2-H_{Ac}/C_4-H_{Bu} ratio of 0.58 and the control group with no Ni/Fe_2O_3 showed a comparatively low molar ratio of C_2-H_{Ac}/C_4-H_{Bu} (0.485), which suggests that the magnitude of C_4-H_{Bu} production is significant ($p = 0.03$), while no significant variation ($p = 0.05$) was observed in C_2-H_{Ac} production. In all these groups, the observed variations in EtOH concentrations were also significant ($p = 0.04$) which increased to 225 mg L^{-1} (at 500 mg L^{-1} of Ni/Fe_2O_3) compared with the control which accounted for 92 mg L^{-1} (no Ni/Fe_2O_3). The reduced degree of electron flow in the presence of EtOH has been reported for the DF system, which also justifies the lowered H_2 yield in this set of experiments.[59] In the DF system, VFAs are the key products of acidification from the ferments of FW.[60,61] The effect of Ni/Fe_2O_3 dosages on H_2 yield and VFA concentration emphasizes the efficacy of catalysts in improved FW fermentation in the DF system. The DF system with an optimal dose not only improves acidification but also results in an improved H_2 yield at

a significant level. We assessed the overall ETS activity and E_h of the microbial population. The observed H_2 yield correlated positively with increased ETS activity, supporting the catalytic role of the Ni/Fe_2O_3 nanoparticles. These findings are consistent with previous studies where the bioconversion of FW led to increased ETS activity and VFA production through syntrophic electron transfer.[62–64] Furthermore, both iron and nickel nanoparticles have been reported to mediate electron transfer between different microbial guilds.[65,66] In the current system, there is significant evidence that Ni/Fe_2O_3 enhances ETS activity, E_h, and VFA production. This suggests that the nanoparticles accelerate electron transfer, thereby increasing the overall H_2 yield in the FW-based DF-system.

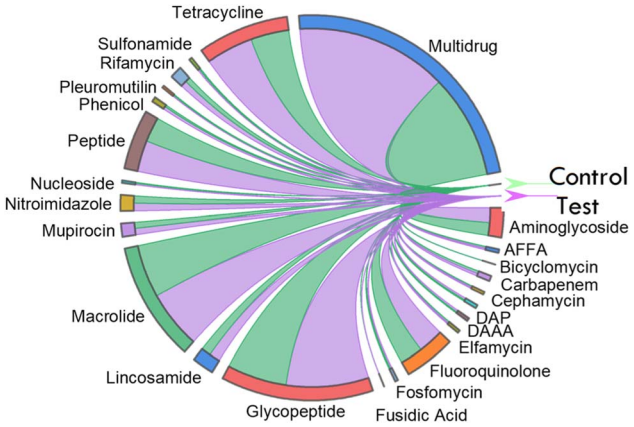

Fig. 4 Abundance and distribution of antibiotic resistance gene (ARG) types in the anaerobic biohydrogen production system. The figure compares the control system (without nanoparticles) to the test system supplemented with Ni/Fe_2O_3. The width of each circular bar is proportional to the total abundance of ARGs in that respective sample.

3.4 Bioinformatics for taxio-metagenomics

Analysis of 16S rRNA gene amplicons, resolved into amplicon sequence variants (ASVs), revealed a statistically significant difference in taxonomic alpha diversity between the naïve control system and the test system supplemented with 200 mg L^{-1} of Ni/Fe_2O_3 (Fig. S3 SI). The taxonomic and alpha diversity regression plot (Fig. S4, SI) revealed the higher abundance-based coverage estimator (ACE) index in the test system, which is supported by the higher Chao1 index. The alpha diversity metrics, including the Shannon (H′) and Simpson indices, along with Pielou's evenness, did not vary significantly between the two samples. A Tukey's HSD test confirmed this, yielding p-values of 0.31 for all three indices Fig. S4 SI. The taxonomic composition from kingdom to species level in observed in the test system, and relative abundance of genus *Clostridium* was dominated in both of the samples (Fig. 3a–f). Highlighting the species-level diversity, *Clostridium beijerinckii*, *Clostridium* LS and *Clostridium chromiireducens* were the major species present in both types of systems, but their proportions were influenced by the presence of Ni/Fe_2O_3. The relative abundance of three Clostridium species increased in the test system compared to the control: *C. beijerinckii* rose from 63.16% to 64.21%, *C.* sp. LS from 2.14% to 2.48%, and *C. chromiireducens* from 1.23% to 1.55%.

The antibiotic resistance gene (ARG) profiles, visualized in a chord diagram, were dominated by multidrug, glycopeptide, macrolide, peptide, and fluoroquinolone resistance genes in both systems, Fig. 4. While 34.3% of ARGs were common to both, the test system showed a significant shift in multidrug and glycopeptide resistance and contained a larger proportion of unique ARGs (39.5%) compared to the control (26.2%).

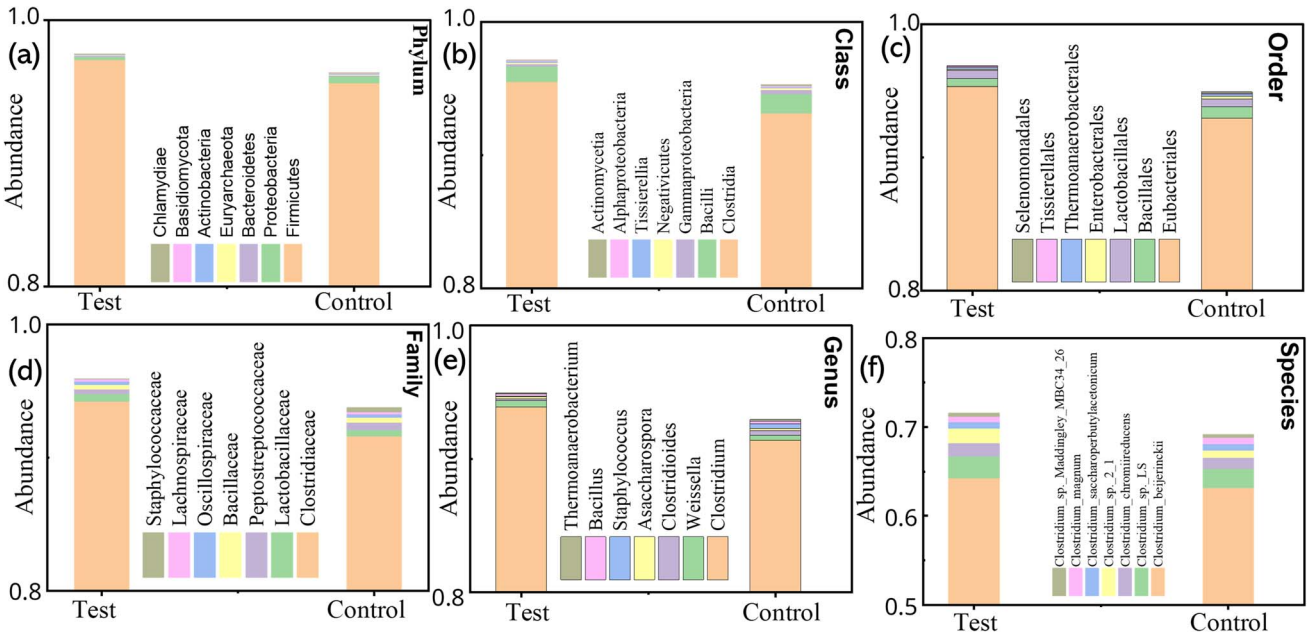

Fig. 3 Taxonomic shifts in the microbial community in response to Ni/Fe_2O_3 supplementation. The figure illustrates changes in community structure at various taxonomic ranks from phylum to species in the biohydrogen production system.

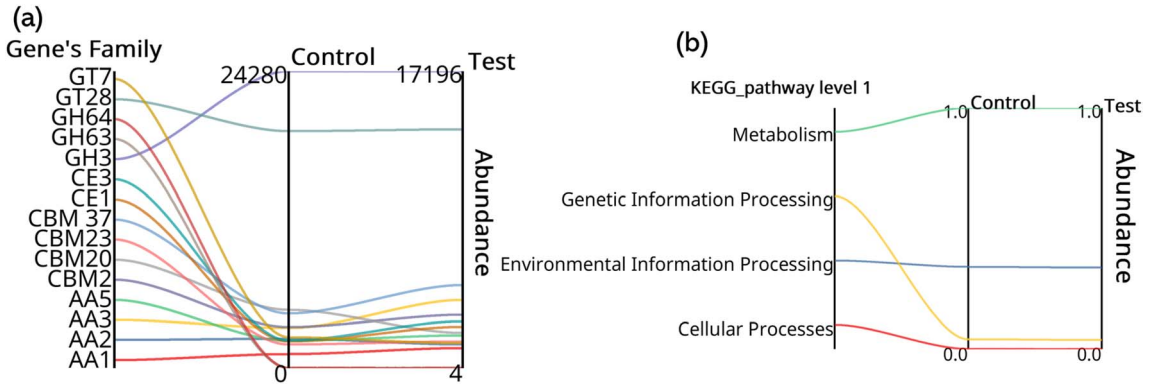

Fig. 5 Functional gene annotation in the anaerobic H_2 production system. Comparison of relative gene abundance for (a) CAZy families and (b) KEGG Level 1 pathways. "Test" samples were augmented with Ni/Fe_2O_3 nanoparticles; "Control" samples were not. All abundance values are normalized (0–1).

Exposure of the microbial population to Ni/Fe_2O_3 catalysts led to an increased abundance of certain ARGs in the test system. Consequently, while the system with the Ni/Fe_2O_3 additive accumulated more of these specific ARGs, this selective pressure may have reduced the overall diversity of ARGs present. The diversity and relative abundance of genes in a metagenome reflect the community's dominant metabolic functions and its characteristic functional profile. The abundance profile of genes encoding Carbohydrate-Active Enzymes (CAZymes), which are crucial for breaking down substrates in the food waste (FW)-based dark fermentation system, is shown in Fig. 5a. The most abundant CAZyme classes were Glycoside Hydrolases

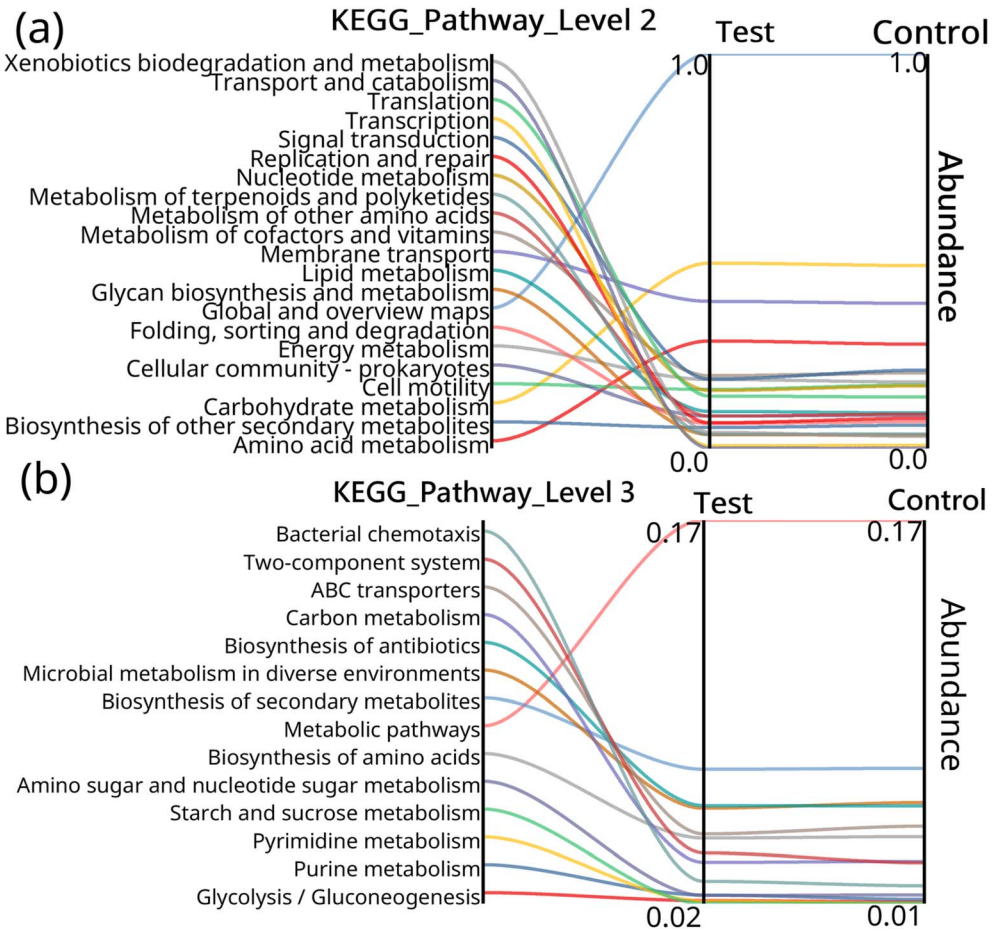

Fig. 6 Relative abundance of genes assigned to KEGG pathways. (a) Functional categories at Level 2 and (b) specific pathways at Level 3. The "test" system contains Ni/Fe_2O_3 nanoparticles, and the "control" does not. Values are normalized from 0 to 1.

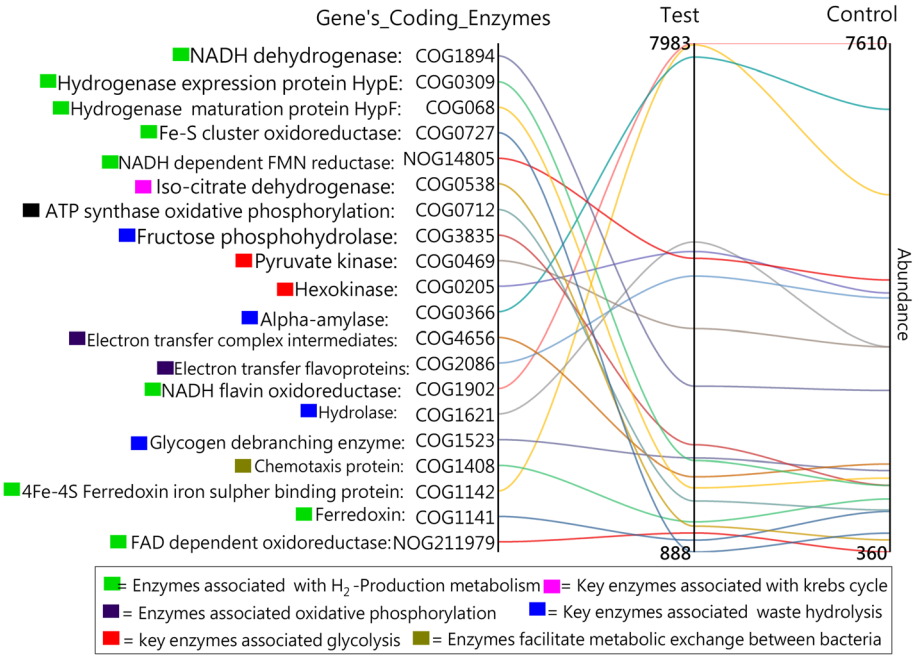

Fig. 7 Parallelograms showing the abundance of the COG and NOG categories for the test and control systems.

(GHs), followed by Glycosyl Transferases (GTs), Polysaccharide Lyases (PLs), Carbohydrate Esterases (CEs), Auxiliary Activities (AAs), and Carbohydrate-Binding Modules (CBMs), Fig. 5a (also refer Fig. S5 SI).

In the parallelograms (Fig. 5a) used for pairwise expression difference in CAZys gene abundance between the test and the control system, the variation in gene abundance is clearly depicted. The results indicate a decrease in the abundance of the GH3 and GT28 families. GH3 enzymes are primarily involved in hydrolyzing cellulose and hemicellulose backbones, while GT28 is associated with intracellular peptidoglycan synthesis. In contrast, there was an enrichment of the CE1 and CE2 families. These hydrolases act on a wide variety of substrates, particularly by removing acetyl groups from xylan. This suggests that Ni/Fe_2O_3 nanoparticles influence the profile of active CAZy enzymes in the FW-based DF-system. These observations are consistent with the results reported in the literature, where the adsorption of ZnO-NPs evidently promotes the abundance level of genes controlling the CAZys system, in particular enzymatic glycosyltransferase, indicating the key role of ZnO-NPs and biosynthetic genes in metabolic processes.[67]

Functional annotation using the KEGG database revealed that "Metabolism", "Genetic Information Processing", "Cellular Processes", and "Environmental Information Processing" were the dominant Level 1 pathway categories in both systems, Fig. 5b. Analysis at KEGG pathway Level 2 revealed differences in the metabolic potential between the two systems, Fig. 6a. Specifically, in the system augmented with Ni/Fe_2O_3 nanoparticles (the "test" system), there was a notable enrichment of genes associated with xenobiotics biodegradation and metabolism, carbohydrate metabolism, membrane transport, and amino acid metabolism. Further analysis at KEGG Level 3 identified specific metabolic pathways with differential abundance between the test and control systems (Fig. 6b). The test system showed a significantly higher abundance of pathways related to xenobiotics biodegradation, carbohydrate metabolism, membrane transport, and amino acid metabolism, confirming that the addition of Ni/Fe_2O_3 directly enhances these functions in the DF-system. These results align with previous findings, such as those by Rui *et al.* (2018), who demonstrated that Fe-NPs enhance amino acid metabolism in *Arachis hypogaea* by stimulating its biological activity.[68] Similar observations were reported by García-Rodríguez *et al.* (2020), who described the role of Fe_2O_3 NPs in accelerating the membrane transport through brush border membrane enzymes such as aminopeptidase-N (observed in this study) and Na^+/K^+ ATPase.[69] Functional analysis of COG/NOG categories showed that Ni/Fe_2O_3 nanoparticles enhanced central metabolism, with an enrichment of genes for glycolysis, the Krebs cycle, and oxidative phosphorylation, Fig. 7. This effect appears to be stimulate these oxido-reductive pathways by upregulating key regulatory components. The evidence for this includes the increased abundance of [4Fe–4S] ferredoxin, iron–sulfur binding proteins, NADH-dependent FMN reductase, hydrogenase maturation proteins (HypE, HypF), and intermediates of the electron transfer metabolism. The NADH pathway is closely related to H_2 production, which is due to pyruvate production from a glucose molecule accompanied by NADH production. The results show a coordinated upregulation of key metabolic enzymes, including hydrolases (*e.g.*, alpha-amylase), solubilization enzymes (*e.g.*, glycogen debranching enzymes), kinases, and oxidoreductases. The enhancement of kinase activity is particularly noteworthy, as iron oxide nanoparticles (like the Ni/

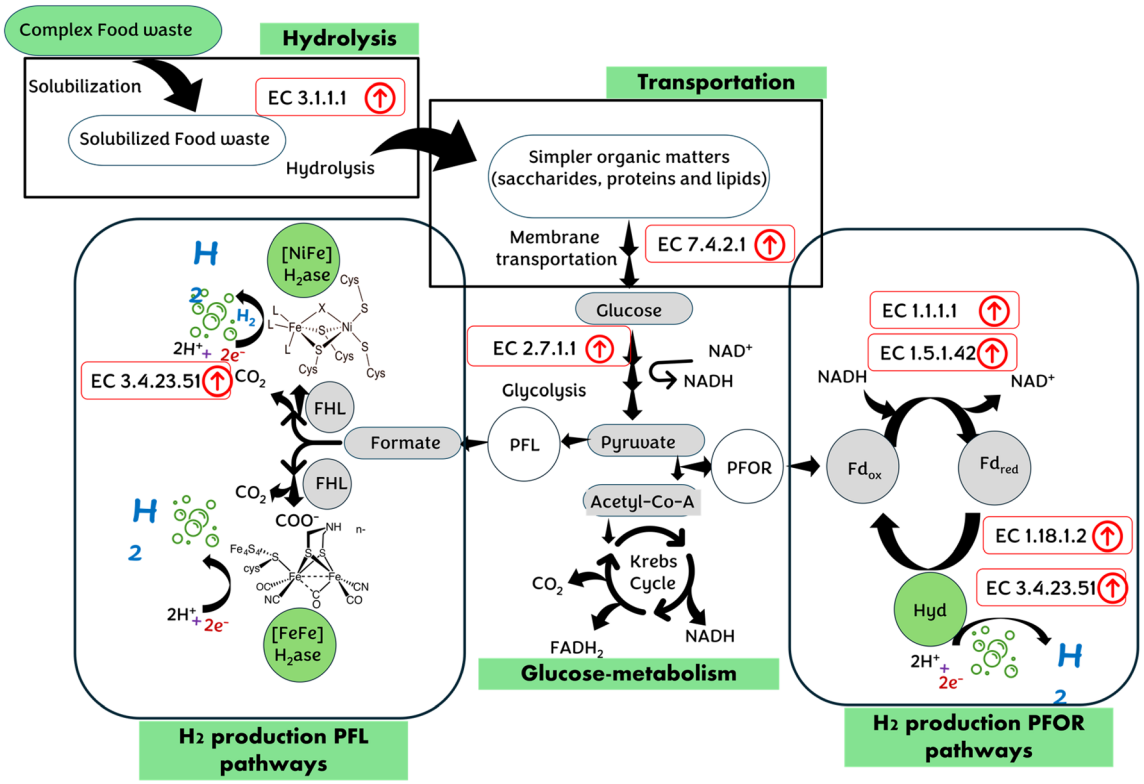

Fig. 8 Proposed mechanism for the impact of Ni/Fe_2O_3-engineered nanoparticles on anaerobic biohydrogen production at the metagenomic level. Red upward arrows indicate the metabolic pathways and genes observed to be upregulated in this study. Ni/Fe_2O_3 is hypothesized to enhance hydrogenesis by stimulating the key enzymatic activities while also triggering microbial stress responses.

Fe_2O_3 composite) have been reported to promote the expression of kinase proteins and influence FAK-mediated signaling pathways.[70] Herein, the dose-dependent catalytic effect of Ni/Fe_2O_3 was observed, where the FW-based DF system with 200 mg L^{-1} of Ni/Fe_2O_3 showed the accessible limit for the microbial communities to interact or improve hydrolysis capability, which later improved the conversion of complex macromolecules to soluble sugars, protein or lipids. This evidences the dose-dependent interaction between the nanocatalysts and the biological system, and could be explained as the intrinsic behavior of Ni/Fe_2O_3 that leads to the optimal physical adsorption[71] and the internalization or intracellular trafficking[72] of ions to the microbial consortium and subsequently increases the overall hydrolysis. Convincingly, the metagenomics analysis leads to a coordinated relationship between Ni/Fe_2O_3 and the metabolic pathway in the microbiota at the molecular level (Fig. 8). The upregulation of some key metabolic activity enzymes suggests a positive deviation from the control sample (no Ni/Fe_2O_3) to the channelized H_2 production in the FW-based DF system.

4. Conclusion

In conclusion, this study demonstrates that a synthesized Ni/Fe_2O_3 nanocatalyst (200 mg L^{-1}, 2.5 nm) significantly enhances H_2 production from FW in a DF-system. The catalyst improved key metabolic processes, including hydrolysis, electron transport, and short-chain fatty acid generation, which collectively favored the hydrogenotrophic pathway. Metagenomic analysis confirmed this functional enhancement at the genomic level, revealing a microbial community dominated by *Clostridium* species. Specifically, the catalyst prompted a functional shift, upregulating genes essential for saccharide hydrolysis, nutrient transport, glycolysis, and NADH/ferredoxin-mediated electron transfer, including the maturation of Ni–Fe hydrogenase. These findings provide novel, genome-level insights into how bimetallic nanocatalysts can effectively modulate microbial metabolism for more efficient DF-systems.

Author contributions

The manuscript was written with the contributions of all the authors.

Conflicts of interest

The authors declare that they have no competing interests.

Data availability

All the data and findings needed to evaluate the conclusions are present in the paper and its supplementary information (SI). Supplementary information is available. See DOI: https://doi.org/10.1039/d5se01709b.

Acknowledgements

The authors acknowledge the support of the Hong Kong Environment and Conservation Fund (127/2022).

References

1 K. He, W. Li, L. Tang, W. Li, S. Lv and D. Xing, *Environ. Sci. Technol.*, 2022, **56**, 11931–11951.
2 P. Mishra, PhD thesis, Universiti Malaysia Pahang, 2018.
3 P. Mishra, PhD Thesis, Universiti Malaysia Pahang, Malaysia, 2018.
4 P. Packiyadhas, S. K. Sivaperumal and S. Murugesan, *J. Mater. Cycles Waste Manag.*, 2025, **27**, 777–795.
5 S. Wang, L. Peng, Y. Jiang, P. Gikas, B. Zhu and H. Su, *Sci. Rep.*, 2016, **6**, 34640.
6 E. B. Agyekum, M. I. Al-Maaitah, P. Kumar, F. Odoi-Yorke and F. L. Rashid, *Energy Convers. Manage.: X*, 2025, **27**, 101111.
7 P. Mishra, D. Johnravindar, J. W. Wong and J. Zhao, *Sustainable Energy Fuels*, 2022, **6**, 5425–5438.
8 J. d. J. s. Montoya-Rosales, A. Ontiveros-Valencia, D. A. Esquivel-Hernández, C. Etchebehere, L. B. Celis and E. Razo-Flores, *Environ. Sci. Technol.*, 2023, **57**, 11552–11560.
9 R. K. Thauer, K. Jungermann and K. Decker, *Bacteriol. Rev.*, 1977, **41**, 100–180.
10 A. P. Sohale, S. Janardanan, D. Yadav, B. Dash and M. D. Yadav, *Ind. Eng. Chem. Res.*, 2023, **62**, 14755–14771.
11 Q. Kang, D. Lai, W. Tang, Q. Lu and F. Gao, *Chem. Sci.*, 2021, **12**, 3818–3835.
12 T. Luo, Q. Xu, W. Wei, J. Sun, X. Dai and B.-J. Ni, *Environ. Sci. Technol.*, 2022, **56**, 3658–3668.
13 B. Karthikeyan and G. Velvizhi, *Int. J. Hydrogen Energy*, 2024, **52**, 536–554.
14 D. Wang, Q. Pan, J. Yang, S. Gong, X. Liu and Y. Fu, *Environ. Sci. Technol.*, 2024, **58**, 2598–2614.
15 T. Manutsyan, S. Blbulyan, A. Vassilian, T. Semashko, G. Kirakosyan, L. Gabrielyan, K. Trchounian and A. Poladyan, *FEMS Microbiol. Lett.*, 2024, **371**, fnad138.
16 Y. Wang, Y. Zhao, S. Wang, G. Xiao, Y. Jin, Z. Wang and H. Su, *ACS Sustain. Chem. Eng.*, 2022, **11**, 300–311.
17 S. Kumar and P. Maiti, *RSC Adv.*, 2016, **6**, 67449–67480.
18 Z. Ji, H. Zhang, H. Liu, O. M. Yaghi and P. Yang, *Proc. Natl. Acad. Sci. U. S. A.*, 2018, **115**, 10582–10587.
19 W. Tu, I. P. Thompson and W. E. Huang, *Proc. Natl. Acad. Sci. U. S. A.*, 2024, **121**, e2404958121.
20 Ö. B. Gökçek and Ş. N. Erdoğmuş, *Int. J. Hydrogen Energy*, 2024, **49**, 337–348.
21 M. Taherdanak, H. Zilouei and K. Karimi, *Int. J. Hydrogen Energy*, 2016, **41**, 167–173.
22 R. Lin, J. Cheng, L. Ding, W. Song, M. Liu, J. Zhou and K. Cen, *Bioresour. Technol.*, 2016, **207**, 213–219.
23 Z. Li, J. Wang, K. Tian, C. Zhou, Y. Pei, J. Zhang and L. Zang, *ACS Omega*, 2022, **7**, 41594–41605.
24 C. Roy, B. Sebok, S. Scott, E. Fiordaliso, J. Sørensen, A. Bodin, D. Trimarco, C. Damsgaard, P. Vesborg and O. Hansen, *Nat. Catal.*, 2018, **1**, 820–829.
25 Q. Zhang, S. Xu, Y. Li, P. Ding, Y. Zhang and P. Zhao, *Fuel*, 2021, **305**, 121585.
26 W. Lubitz, H. Ogata, O. Rudiger and E. Reijerse, *Chem. Rev.*, 2014, **114**, 4081–4148.
27 J. Yang, H. Zhang, H. Liu, J. Zhang, Y. Pei and L. Zang, *Bioresour. Technol.*, 2022, **351**, 127027.
28 P. Mishra, I. R. Akaniro, R. Zhang, P. Wang, Y. Geng, D. Li, Q. Xu, J. W. Wong and J. Zhao, *ACS ES&T Eng.*, 2024, **4**(10), 2424–2434.
29 F. Ndayisenga, Z. Yu, B. Wang, G. Wu and H. Zhang, *Energy Convers. Manage.: X*, 2024, **22**, 100541.
30 B. Xiao and J. Liu, *Chin. Sci. Bull.*, 2009, **54**, 2038–2044.
31 A. S. Oberoi, S. Sriram and J. W. Wong, *Int. J. Hydrogen Energy*, 2024, **67**, 566–576.
32 W. Xiu, M. Wu, S. L. Nixon, J. R. Lloyd, N. M. Bassil, R. Gai, T. Zhang, Z. Su and H. Guo, *Environ. Sci. Technol.*, 2022, **56**, 10105–10119.
33 A. P. H. Association, *Standard Methods for the Examination of Water and Wastewater*, American public health association, 1926.
34 M. Gong, Y. Li, H. Wang, Y. Liang, J. Z. Wu, J. Zhou, J. Wang, T. Regier, F. Wei and H. Dai, *J. Am. Chem. Soc.*, 2013, **135**, 8452–8455.
35 J. Alsarraf, A. A. Al-Rashed, A. A. Alnaqi and A. S. Goldanlou, *Powder Technol.*, 2021, **379**, 537–546.
36 M. W. Louie and A. T. Bell, *J. Am. Chem. Soc.*, 2013, **135**, 12329–12337.
37 H. Liang, M. Xu, Y. Bu, B. Chen, Y. Zhang, Y. Fu, X. Xu and J. Zhang, *Appl. Surf. Sci.*, 2019, **485**, 64–69.
38 Q. Luo, Y. Zhao, L. Sun, C. Wang, H. Xin, J. Song, D. Li and F. Ma, *Chem. Eng. J.*, 2022, **437**, 135376.
39 A. P. Grosvenor, M. C. Biesinger, R. S. C. Smart and N. S. McIntyre, *Surf. Sci.*, 2006, **600**, 1771–1779.
40 P. Dubey, N. Kaurav, R. S. Devan, G. Okram and Y. Kuo, *RSC Adv.*, 2018, **8**, 5882–5890.
41 T. Yamashita and P. Hayes, *Appl. Surf. Sci.*, 2008, **254**, 2441–2449.
42 P. Li, Y. Xuan, B. Jiang, S. Zhang and C. Xia, *Electrochem. Commun.*, 2022, **134**, 107188.
43 L. Sun, C. H. Hendon, S. S. Park, Y. Tulchinsky, R. Wan, F. Wang, A. Walsh and M. Dincă, *Chem. Sci.*, 2017, **8**, 4450–4457.
44 T. Raj, K. Chandrasekhar, R. Morya, A. K. Pandey, J.-H. Jung, D. Kumar, R. R. Singhania and S.-H. Kim, *Bioresour. Technol.*, 2022, **360**, 127512.
45 S. Eduok, B. Martin, R. Villa, A. Nocker, B. Jefferson and F. Coulon, *Ecotoxicol. Environ. Saf.*, 2013, **95**, 1–9.
46 P. Szczyglewska, A. Feliczak-Guzik and I. Nowak, *Molecules*, 2023, **28**, 4932.
47 L. Zhu, H. Tao, X. Dai, B. Dong and W. Zhang, *J. Environ. Manage.*, 2023, **326**, 116722.
48 Q. Wang, K. Feng and H. Li, *Bioresour. Technol.*, 2020, **315**, 123804.
49 N. Srivastava, A. Hussain, D. Kushwaha, S. Haque, P. Mishra, V. K. Gupta and M. Srivastava, *Fuel*, 2021, **304**, 121391.

50 R. Posmanik, C. M. Martinez, B. Cantero-Tubilla, D. A. Cantero, D. Sills, M. J. Cocero and J. W. Tester, *ACS Sustain. Chem. Eng.*, 2018, **6**, 2724–2732.
51 C.-A. Aceves-Lara, E. Latrille, T. Conte and J.-P. Steyer, *Water Sci. Technol.*, 2012, **65**, 1281–1289.
52 P. Chen, Y. Wang, L. Yan, Y. Wang, S. Li, X. Yan, N. Wang, N. Liang and H. Li, *Biol. Res.*, 2015, **48**, 1–8.
53 T.-H. Kim, D. Song, Y.-J. Jeon, O. Hwang, J.-Y. Nam and Y.-M. Yun, *Chem. Eng. J.*, 2023, **476**, 146520.
54 K. Ma, H. Zhao, C. Zhang, Y. Lu and X.-H. Xing, *Int. J. Hydrogen Energy*, 2012, **37**, 15875–15885.
55 S. Zhang, X. Zhang, Y. Yuan, K. Li and H. Liu, *Sci. Total Environ.*, 2023, **855**, 158911.
56 S. Srikanth and S. V. Mohan, *RSC Adv.*, 2012, **2**, 6576–6589.
57 V. Schirrmacher, *Biomedicines*, 2020, **8**, 526.
58 F. Monlau, E. Trably, A. Barakat, J. Hamelin, J.-P. Steyer and H. Carrere, *Environ. Sci. Technol.*, 2013, **47**, 12591–12599.
59 W. Li, Q. Zhang, J. Liu, N. Ren, X. Zeng and Y. Jia, *Chem. Eng. J.*, 2023, **474**, 145997.
60 G. Mohanakrishna, N. P. Sneha, S. M. Rafi and O. Sarkar, *Sci. Total Environ.*, 2023, **888**, 163801.
61 M. Du, X. Liu, C. Li, S. Long, L. Luo, Y. Guo and D. Wang, *ACS ES&T Eng.*, 2023, **3**, 1986–1996.
62 J. Yang, Y.-B. Sim, H.-H. Joo, O. Mašek and S.-H. Kim, *Int. J. Hydrogen Energy*, 2024, **53**, 1293–1302.
63 J. Bu, H.-L. Wei, Y.-T. Wang, J.-R. Cheng and M.-J. Zhu, *Water Res.*, 2021, **202**, 117440.
64 Q. Jiang, Y. Chen, S. Yu, R. Zhu, C. Zhong, H. Zou, L. Gu and Q. He, *Chem. Eng. J.*, 2020, **398**, 125643.
65 Y. Zhu, Z. Zhao, Y. Yang and Y. Zhang, *Waste Manage.*, 2020, **118**, 481–490.
66 C. G. Camacho and B. Ruggeri, *Chem. Eng. Trans.*, 2018, **64**, 391–396.
67 M. Xiao, A. Li, X. Zhang and B. Ji, *J. Clean. Prod.*, 2024, **447**, 141509.
68 M. Rui, C. Ma, J. C. White, Y. Hao, Y. Wang, X. Tang, J. Yang, F. Jiang, A. Ali and Y. Rui, *Environ. Sci.: Nano*, 2018, **5**, 2088–2102.
69 A. García-Rodríguez, F. Moreno-Olivas, R. Marcos, E. Tako, C. N. Marques and G. J. Mahler, *Environ. Sci.: Nano*, 2020, **7**, 3940–3964.
70 S. J. Soenen, N. Nuytten, S. F. De Meyer, S. C. De Smedt and M. De Cuyper, *Small*, 2010, **6**, 832–842.
71 X. Duan and Y. Li, *Small*, 2013, **9**, 1521–1532.
72 F. Zhao, Y. Zhao, Y. Liu, X. Chang, C. Chen and Y. Zhao, *Small*, 2011, **7**, 1322–1337.